Effects of Catalyst Activity Profiles on Polyethylene Reactor Dynamics

Gary J. Wells and W. Harmon Ray
Dept. of Chemical Engineering, University of Wisconsin-Madison, Madison, WI 53706

Juraj Kosek
Dept. of Chemical Engineering and Center for Nonlinear Dynamics, Prague Institute of Chemical Technology, Technicka 5, 16628 Prague 6, Czech Republic

The dynamics and stability characteristics of slurry loop and tank reactors were studied using continuation analysis to examine the effects of catalyst activity profiles on reactor dynamics. The production of high-density polyethylene through the copolymerization of ethylene with hexene was studied using catalysts of the decay type (for example, $TiCl_4$ on silica, or other Ziegler-Natta catalysts) and the buildup-type (for example, chromium oxide catalysts on silica of the Phillips type). Sustained oscillations were found to exist for decay-type catalysts in loop reactors. For both tank and loop reactors, the buildup-type catalyst exhibited isolated solution branches (isola) and multiplicity phenomena in addition to sustained oscillations. The sigmoidal shape of the buildup-type catalyst rate curve is postulated as the reason for the additional multiplicity and isola phenomena. The implications for industrial operating conditions are discussed.

Introduction

As early as 1918, Liljenroth showed that chemical reactors for oxidizing ammonia could exhibit interesting nonlinear phenomena such as multiple steady states and instabilities (Liljenroth, 1918). The cause of these phenomena was shown to be the interaction of the mass and energy balances of the reactive system. Much subsequent research has shown that the nonlinear interaction of mass- and energy-balance equations can also cause other dynamic phenomena, such as oscillatory states, isolated steady-state solution branches, and traveling waves, especially in polymerization reactors (Ray and Villa, 2000). The presence of these phenomena has serious implications for the operation, design, and control of chemical reactors.

For catalyzed systems, the degree of coupling between the mass and energy balances is often governed by the catalyst activity profile during its residence time in the reactor. Thus, it is of interest to study the effect of this profile on reactor dynamics. In the current work, the catalyzed production of high-density polyethylene (HDPE) polymer in slurry loop and tank reactors is considered, and commercial catalysts representing two extremes of activity characteristics are explored.

Correspondence concerning this article should be addressed to W. Harmon Ray.

In addition to providing a realistic case study of reactor dynamics, the examination of the HDPE production system is motivated by several other factors. The analysis of dynamic behavior is especially interesting in polymer reactors, since polymer properties are highly dependent on reactor dynamics. Also, polymerization reactions are often highly exothermic, leading to a high degree of coupling between the mass and energy balances. Various types of nonlinear phenomena are known to exist for similar polymer systems using a $TiCl_4$-on-silica catalyst in fluidized-bed reactors (Choi and Ray, 1985; Hyanek et al., 1995), gas-phase stirred beds (Choi and Ray, 1988; Gorbach et al., 2000), and bulk polypropylene loop reactors (Zacca and Ray, 1993; Hyanek et al., 1995). Also, using a detailed model of the mass- and energy-transport equations, Kosek and Ray showed that multiple steady states and oscillations can occur in slurry loop reactors for olefin polymerization (Kosek and Ray, 1999). However, nothing has been published comparing the dynamic effects of different catalysts.

Industrial HDPE production processes

High-density polyethylene (HDPE), used to produce a wide variety of products such as plastic bottles and piping, is a

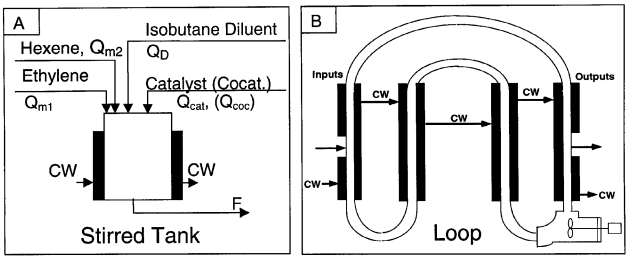

Figure 1. Stirred-tank (A) and loop (B) processes considered for HDPE production.

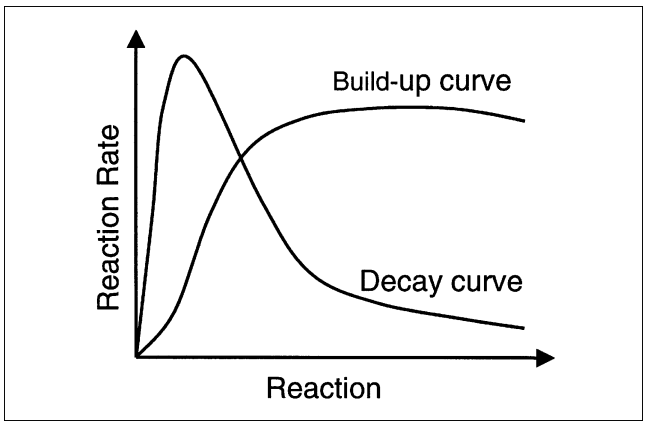

Figure 2. "Buildup" and "decay" catalyst activity profiles.

product of great industrial importance. About 6.3 billion kg were produced in the United States alone in 1999 (Storck et al., 2000). Typically, the processes for the production of HDPE involve the use of transition-metal catalysts. The two most common catalysts used for the processes involved are summarized below (Debling et al., 1994; Kissin, 1996):

Processes Catalyzed by Chromium Oxide on Silica (Phillips Processes). These processes are usually operated in fluidized-bed, slurry-tank, or slurry loop reactors.

Processes Using Ziegler-Natta Catalysts. These processes usually use titanium chloride ($TiCl_4$) on silica, and they operate in solution, fluidized-bed, slurry-tank, or slurry-loop reactors.

The current study compares the nonlinear dynamic behavior of HDPE production using each of these catalyst systems through the copolymerization of ethylene with hexene in slurry. Tubular loop and tank reactors are considered; these types of reactors are shown in Figure 1. For these reactors, both catalyst systems operate at relatively low pressures between 20 and 30 atm. Production typically occurs with catalyst residence times of about 0.5–2 h and temperatures from 80°C to 120°C. For loop reactors, the reactor volume is about 100 m^3, while ethylene monomer conversion is usually high, ranging from 95% to 98% (Zacca, 1995). Tank reactors typically have about one-half to one-third the amount of heat-transfer area per unit-reactor volume as loop reactors (Chandrasekhar et al., 1988). Consequently, the maximum productivity per unit volume is lower in tank reactors than in loop reactors.

Reaction Kinetics

Types of catalyst activity profiles

The chemical reaction mechanisms for catalyst activation, initiation, polymerization, and deactivation determine the qualitative and quantitative nature of the catalyst-activity curves. Two major types of catalyst-activity profiles exist for the production of HDPE: a "buildup" type and a "decay" type (Keii, 1972). Note that the catalyst-activity profile appears as a reaction-rate curve when temperature and monomer concentrations are maintained constant with time. These profiles are given in Figure 2. The buildup type of catalyst reaction-rate curve typically results from a delay in activation of the catalyst and a slower deactivation. When chromium oxide catalysts are used without cocatalyst, such a delay in activation occurs, and the system exhibits the buildup-type rate curve. The decay-type rate curve is typically the result of rapid activation and subsequent deactivation. For $TiCl_4$ catalysts on silica, the addition of a triethyl aluminum cocatalyst causes rapid activation followed by deactivation. Thus, these catalyst systems exhibit the decay-type rate curve. The qualitatively different kinetic mechanisms of the chromium oxide and titanium chloride catalysts systems are presented in the following section.

Copolymerization using a titanium chloride catalyst

The effectiveness of titanium chloride catalysts for the polymerization of olefins was originally discovered by Ziegler and Natta (Ziegler, 1955; Natta, 1955). These catalysts are often deposited on a support material and are mixed with metal alkyl cocatalysts such as triethyl aluminum. It is widely believed that catalyst sites of various activities exist due to surface morphology and titanium oxidation state. Since only the $+2$ and $+3$ oxidation states of Ti are believed to be active in polymerizing ethylene (Kashiwa and Yoshitake, 1984), a two-site model is often used for simulation purposes. This approach is employed in the current study. Other steps in the ethylene polymerization process, such as chain initiation, propagation, chain-transfer, and catalyst deactivation are also considered. Since detailed site-transformation reactions and chain-transfer reactions with the diluent are not likely to be significant in determining dynamic behavior, these reactions are not modeled here. All reaction steps considered in this study are summarized in Table 1. Based on this kinetic model, the corresponding system of differential balance equations describing HDPE production using $TiCl_4$ catalysts on silica in a perfectly mixed slurry-tank reactor is given in Table 2.

Using this kinetic mechanism and a simple semibatch model, rate constants were chosen to fit experimental data measured by Calabro and Lo for the slurry polymerization of ethylene (Calabro and Lo, 1988). These data and the model fit are presented in Figure 3, and the kinetic parameters used in this study are presented in Table 3. The parameters, chosen from the literature and adjusted to fit the specific rate curve, are thought to be representative of this family of catalysts. An Arrhenius expression for the temperature dependence of the rate constants is used. A partition coefficient

was used to determine the monomer and comonomer concentrations available for reaction at the catalyst site based on concentrations in the bulk slurry.

Copolymerization using a chromium oxide catalyst on silica

As in the case of titanium chloride, the activation of chromium oxide catalysts for ethylene polymerization has several stages involving the metal oxidation state. Oxidation states ranging from +6 to +2 are known to exist for the chromium atom in chromium oxides. There has been much debate about the oxidation state of the active site for ethylene polymerization, but there is strong evidence that, in the absence of cocatalyst, a sequence of reduction reactions involving the ethylene monomer must occur to allow chain growth to proceed (McDaniel, 1985). In the current study, two oxidation-state exchanges followed by site activation and initiation are assumed to occur before propagation. The complete reaction-mechanism model for the copolymerization of ethylene using chromium oxide is given in Table 4. The corresponding reactor equations for polymerization in a perfectly stirred slurry-tank reactor are given in Table 5.

It should be noted that for the chromium active center concentrations (C_1^*, C_2^*, and C_3^*), the subscripted numbers are used to distinguish between different catalyst oxidation states. However, since knowledge of intermediate species is not required for dynamic analysis, and a detailed understanding of the active chromium center is incomplete, no assumption is made about the *specific* valence states of the chromium atom. Chain transfer to hydrogen is not very effective for many chromium oxide catalysts (Hogan et al., 1981), and does not affect reaction rate; thus it is not modeled here.

Using the chromium oxide-catalyzed slurry polymerization data from McDaniel and Martin (1991), kinetic parameters based on the chemical mechanisms of Table 4 were determined. The model fit and experimental rate data are compared in Figure 4. The kinetic constants used for the model fit are given in Table 6. These parameters were chosen from the best available information and adjusted to fit the specific rate curve. It is believed that the model parameters of this study provide a sufficient description of the catalyst activity profile to allow meaningful analysis of chemical-reactor dynamics.

Table 1. Chemical Reactions Considered for Polymerization of Ethylene Using $TiCl_4$ Catalysts on Silica*

Site activation	
$C_{pot} + C_{cocat} \xrightarrow{k^k_{act,cocat}} P^k_0 + C_B$	(By Cocatalyst)
$C_{pot} + M_i \xrightarrow{k^k_{act,M_i}} P^k_0$	(By Monomer i)**
Chain initiation	
$P^k_0 + M_i \xrightarrow{k^k_{init,M_i}} P^k_{1,i}$	
Chain propagation	
$P^k_{n,E_j} + M_i \xrightarrow{k^k_{p,M_i,E_j}} P^k_{n+1,E_i}$	
Chain transfer	
$P^k_{n,E_j} + C_H \xrightarrow{k^k_{tr,H,E_j}} D^k_{n,E_j} + P^k_0$	(To Hydrogen)
$P^k_{n,E_j} + C_{cocat} \xrightarrow{k^k_{tr,H,E_j}} D^k_{n,E_j} + P^k_0$	(To Cocatalyst)
$P^k_{n,E_j} \xrightarrow{k^k_{tr,sp,E_j}} D^k_{n,E_j} + P^k_0$	(Spontaneous)
$P^k_{n,E_j} + M_i \xrightarrow{k^k_{tr,M_i,E_j}} D^k_{n,E_j} + P^k_{1,E_i}$	(To Monomer)
Site deactivation	
$P^k_0 \xrightarrow{k_{spd}} C_d$	
$P^k_{n,E_j} \xrightarrow{k_{spd}} C_d + D^k_{n,E_j}$	(Spontaneous)

*Symbols for species concentrations (e.g., C_H for the concentration of H_2) are used to allow a common nomenclature in formulating the balance equations of Table 2. The only difference in nomenclature between Tables 1 and 2 is that the length of growing polymer chains is not considered for balance equations.

**Note: $i = 1$ is ethylene; $i = 2$ is 1-hexene. Only activation by 1-hexene is considered.

Reactor Modeling

In this study, both tubular loop and tank reactors are considered for HDPE production. Loop reactors usually operate at high recirculation rates that allow them to be modeled as a stirred-tank reactor (Murakami et al., 1982; Zacca and Ray, 1993). Thus, both the loop and tank systems considered in this work can be modeled using the tank-model equations summarized in Tables 2 and 5. From a modeling standpoint, the major difference between the loop and tank reactors is the heat-transfer area per volume. Plant-scale tank reactors typically have a heat-transfer area per unit volume of 10–20 cm^2/L, while for tubular loop reactors, the area is about 2–3 times as much (Chandrasekhar et al., 1988). Also, the heat transfer coefficient is higher in a loop reactor due to higher velocities at the heat transfer surface. A constant temperature difference between the reactor contents and coolant is assumed, and can be thought of as the log-mean temperature difference. Since there is little temperature variation around a loop reactor with high recycle rates, this representation is reasonable.

Model parameters and process constraints

For the simulations performed in this study, several design parameters were held constant, and are given in Table 7. The feed concentrations of ethylene and hexene are the saturation values at an operating pressure of 30 atm, and were computed using the Benedict-Webb-Rubin equation of state. If not otherwise stated, simulation results were obtained using a coolant at 25°C, to be consistent with typical cooling-water temperatures. However, it should be noted that some operations of HDPE production catalyzed by chromium oxide on silica use much higher coolant temperatures, up to about 80°C, due to tight product quality constraints (Norwood, 1966). The use of such high coolant temperatures will be considered near the end of this article. The heat capacity (C_p) and density (ρ) of the slurry mixture were calculated from the component weight fractions (w_i) and the pure-component properties ($C_{p,i}$ and ρ_i) using the mixing rules given in Eqs. 1 and 2.

$$C_p = \sum_{\text{all components } i} w_i C_{p,i} \qquad (1)$$

Table 2. Balance Equations for HDPE Production Catalyzed by $TiCl_4$ on Silica in a Perfectly Mixed Slurry-Tank Reactor

$C_{\text{pot}} = C_{\text{cat}} E_{\text{cat}} \frac{WFMe}{MWMe} - C_d - \sum_i \sum_k (P^k_{\text{act},E_i} + P^k_0)$	(C_{pot} Definition)
$f_{\text{sorpt}} = \frac{C_{M_i,\text{effective}}}{C_{M_i}}$	(f_{sorpt} Definition)
$\frac{dC_{\text{cat}}}{dt} = \frac{f_{\text{cat,feed}}\,\rho}{\tau} - \frac{1}{\tau} C_{\text{cat}}$	(Catalyst)
$\frac{dC_d}{dt} = \frac{\rho f_{\text{cat,feed}} f_{\text{dead,cat}} E_{\text{cat}}}{\tau} \frac{WFMe}{MWMe} - \frac{1}{\tau} C_d + \sum_k \left(k_{spd} \sum_i (P^k_{\text{act},E_i} + P^k_0) \right)$	(Dead Catalyst)
$\frac{dC_{\text{cocat}}}{dt} = \frac{f_{\text{coc,feed}}\,\rho}{\tau M_{\text{cocat}}} - \frac{1}{\tau} C_{\text{cocat}} - C_{\text{cocat}} f_{\text{sorpt}} \sum_k \sum_i \mathrm{k}^k_{\text{tr,cocat},E_i} P^k_{\text{act},E_i} - C_{\text{cocat}} f_{\text{sorpt}} \sum_k (k^k_{\text{act,cocat}} C_{\text{pot}})$	(Cocatalyst)
$\frac{dP^k_0}{dt} = \frac{f_{\text{cat,feed}} f^k_{0,\text{feed}}\,\rho E_{\text{cat}}}{\tau} \frac{WFMe}{MWMe} - \frac{1}{\tau} P^k_0 - P^k_0 \sum_i k^k_{\text{init},\,M_i} C_{M_i} f_{\text{sorpt}}$ $+ C_{\text{pot}} \left(k^k_{\text{act,cocat}} C_{\text{cocat}} f_{\text{sorpt}} + \sum_i k^k_{\text{act},M_i} C_{M_i} f_{\text{sorpt}} \right) - k_{spd} P^k_0$ $+ \sum_i P^k_{\text{act},E_i} (k^k_{tr,H,E_i} (C_H f_{\text{sorpt}})^{0.5} + k^k_{\text{tr,cocat},E_i} C_{\text{cocat}} f_{\text{sorpt}} + k^k_{\text{tr},sp,E_i})$	(Vacant Sites)
$\frac{dP^k_{\text{act},E_i}}{dt} = -\frac{1}{\tau} P^k_{\text{act},E_i} - P^k_{\text{act},E_i} \left(\begin{array}{l} \sum_{j \neq i} \left(k^k_{p,M_j,E_i} C_{M_j} f_{\text{sorpt}} + k^k_{\text{tr},M_j,E_i} C_{M_j} f_{\text{sorpt}} \right) \\ + k^k_{\text{tr},H,E_i} C_H f_{\text{sorpt}} + k^k_{\text{tr,Cocat},E_i} C_{\text{Cocat}} f_{\text{sorpt}} + k_{\text{spd}} \end{array} \right)$ $+ \sum_{j \neq i} P^k_{\text{act},E_j} f_{\text{sorpt}} (k^k_{p,M_i,E_j} C_{M_i} + k^k_{\text{tr},M_i,E_j} C_{M_i}) + P^k_0 k^k_{\text{init},M_i} C_{M_i} f_{\text{sorpt}}$	(Growing Chains)
$\frac{dC_{M_i}}{dt} = \frac{f_{M_i,\text{feed}}\,\rho}{\tau M_{M_i}} - \frac{1}{\tau} C_{M_i} - C_{M_i} f_{\text{sorpt}} \sum_k k^k_{\text{act},M_i} C_{\text{pot}} - C_{M_i} f_{\text{sorpt}} \sum_k \left(\sum_j k_{p,M_i,E_j} P^k_{\text{act},E_j} + \sum_j k^k_{\text{tr},M_i,E_j} P^k_{\text{act},E_j} \right)$ $- C_{M_i} f_{\text{sorpt}} \sum_k k^k_{\text{init},M_i} P^k_0$	(Monomer)
$\frac{dC_H}{dt} = \frac{f_{\text{H,feed}}\,\rho}{\tau M_H} - \frac{1}{\tau} C_H - (C_H f_{\text{sorpt}})^{0.5} \sum_i \sum_k k^k_{\text{tr},H,E_i} P^k_{\text{act},E_i}$	(Hydrogen)
$\frac{dT}{dt} = \frac{C^{\text{feed}}_p}{C_p \tau} (T_{\text{feed}} - T_{\text{ref}}) - \frac{1}{\tau} (T - T_{\text{ref}}) - \frac{hA}{\rho C_p V} (T - T_c)$ $- \frac{1}{\rho C_p} \sum_i \sum_j \sum_k \Delta H_{\text{poly},M_i} k^k_{p0,M_i,E_j} \exp \left(\frac{-E^k_{A,M_i,E_j}}{RT} \right) P^k_{\text{act},E_j} C_{M_i} f_{\text{sorpt}}$	(Energy)

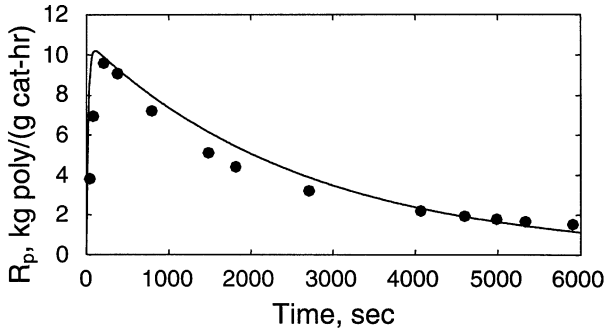

Figure 3. Comparison of model prediction to data of Calabro and Lo (1988) for polyethylene production with a $TiCl_4$ catalyst on silica.

The fit represents a catalyst half-life of about 20 min.

$$\frac{1}{\rho} = \sum_{\text{all components } i} \frac{w_i}{\rho_i}. \tag{2}$$

Third-order polynomials in temperature were used for pure-component heat capacities and densities, and the coefficients of these polynomials are given in Table 8. Note that the catalyst and cocatalyst species are present only in small amounts, and their pure-component contributions to the density and heat capacity are taken to be those of the diluent.

When modeling HDPE production in slurry loop and tank reactors, several process constraints must be considered. The diluent considered in this work is isobutane, a low-boiling alkane common in industrial practice. At a pressure of 30 atm, the boiling point of this diluent is 123°C Lemmon et al., 1998). Also, the melting point of the polymer produced is about 136°C (Osswald and Menges, 1995). Both of these process constraints are rigid for the processes considered, and exceeding them would cause serious upsets in operation. Other constraints can also play a role in certain cases. Fouling of tubes due to low polymer solubility or polymer softening in certain loop-reactor designs can occur at temperatures above about 110°C (Hogan et al., 1981; Benham et al., 1991). For cases with low conversion to polymer, the boiling point of the mixture can be lower than that of pure isobutane, causing difficulties due to bubble formation in the slurry.

It should be noted that the model presented is not valid for predicting behavior at temperatures exceeding these process constraints. However, the goal of this work is not to predict

Table 3. Kinetic Parameters for HDPE Production Using $TiCl_4$ Catalysts on Silica*

Activation Energies (cal/mol)	Site 1	Site 2
Chain transfer	14,000	14,000
Deactivation	12,000	12,000
All others	9,000	9,000
Preexponential Factors	**Site 1**	**Site 2**
Site activation (L/mol-s)		
By cocatalyst	7.0×10^7	7.0×10^7
Chain initiation (L/mol-s)		
By ethylene	2.7×10^6	2.7×10^6
By hexene	3.8×10^5	3.8×10^5
Chain propagation (L/mol-s)		
By ethylene, ethylene end group	7.0×10^8	7.0×10^8
By ethylene, hexene end group	6.0×10^8	6.0×10^8
By hexene, ethylene end group	3.5×10^6	2.3×10^7
By hexene, hexene end group	2.4×10^6	9.8×10^6
Chain transfer		
By hydrogen, ethylene end group [$L^{0.5}/(mol^{0.5}\cdot s)$]	3.0×10^7	3.2×10^8
By cocatalyst, ethylene end group [$L/(mol\cdot s)$]	6.0×10^5	3.0×10^6
Spontaneous, ethylene end group (s^{-1})	2.8×10^2	2.8×10^2
By ethylene, ethylene end group [$L/(mol\cdot s)$]	6.0×10^5	6.0×10^5
By hexene, ethylene end group [$L/(mol\cdot s)$]	1.6×10^5	3.2×10^6
By hydrogen, hexene end group [$L/(mol\cdot s)$]	3.0×10^7	3.2×10^8
By cocatalyst, hexene end group [$L/(mol\cdot s)$]	1.3×10^6	6.0×10^5
Spontaneous, hexene end group (s^{-1})	2.8×10^2	2.8×10^2
By ethylene, hexene end group [$L/(mol\cdot s)$]	6.0×10^5	6.0×10^5
By hexene, hexene end group [$L/(mol\cdot s)$]	1.0×10^7	1.6×10^8
Site deactivation (s^{-1})		
Spontaneous	5,000	5,000

*Rate-constant parameters for site activation, propagation, and site deactivation were chosen to fit the data of Calabro and Lo (1988). Chain initation and chain-transfer constants were taken from Takeda and Ray (1999).

such behavior, but rather to determine the conditions that cause these constraints to be exceeded. The current model is capable of predicting such conditions.

Numerical analysis

To examine the nonlinear dynamic behavior of the systems considered, continuation analyses were performed using the numerical package AUTO (Doedel, 1981). This package uses a pseudoarclength algorithm to analyze the effect of continuation parameters. To provide the bifurcation analysis software with initial steady states, NLEQ was used (Nowak and Weimann, 1991). The stability and qualitative nature of solutions were examined for a variety of cases, and dynamic simulations were performed using the DASSL package (Petzold, 1982).

Both single-parameter and two-parameter bifurcation analyses were performed. The heat-transfer area per unit volume, reactor residence time, and catalyst feed fraction were the major bifurcation parameters used. When used as a bifurcation parameter, the residence time (τ_{in}) was defined as the ratio of the reactor volume (V) to the inlet volumetric flow rate (Q_{in}). As shown in Eq. 3, τ_{in} can be related to a residence time referenced to the *exit* volumetric flow rate (τ) by the ratio of the reaction mixture density (ρ) to that of the feed (ρ_{in}):

$$\tau = \tau_{\text{in}} \frac{\rho}{\rho_{\text{in}}}. \tag{3}$$

When considering simulations explaining the effect of catalyst feed fraction, we should note that this parameter affects reactor dynamics only inasmuch as it defines the number of potentially active sites fed to the reactor. The effect of the catalyst on dynamics is defined through the *shape* of the catalyst-activity profile. Thus, if we use a catalyst of different activity, but with the same profile shape, the same dynamic phenomena will occur, but they will occur for different values

Table 4. Chemical Reactions Considered for Polymerization of Ethylene Using Chromium Oxide Catalysts on Silica*

Oxidation state exchange

$$C_1^* + M_i \xrightarrow{k_{st,M_i,1}} C_2^*$$

$$C_2^* + M_i \xrightarrow{k_{st,M_i,2}} C_3^*$$

Site activation

$$C_3^* + M_i \xrightarrow{k_{\text{act},M_i}} P_0^*$$

Chain initiation

$$P_0^* + M_i \xrightarrow{k_{\text{ini},M_i}} P_{E_i,1}^*$$

Chain propagation

$$P_{E_j,n}^* + M_i \xrightarrow{k_{p,M_i,E_j}} P_{E_i,n+1}^*$$

Spontaneous catalyst decay

$$C_i^*, P_0^*, P_{E_j,n}^* \xrightarrow{k_{spd}} C_d, D_{E_j,n}$$

*Symbols for species concentrations are used to allow a common nomenclature to be used in formulating the balance equations of Table 5; the only exception to this common nomenclature is that polymer chain lengths are not distinguished in balance equations.

Table 5. Balance Equations for HDPE Production Catalyzed by Chromium Oxide on Silica in a Perfectly Mixed Slurry Tank Reactor

$f_{\text{sorpt}} = \dfrac{C_{\boldsymbol{M}_i,\text{effective}}}{C_{M_i}}$	(f_{sorpt} definition)
$\dfrac{dC_{\text{cat}}}{dt} = \dfrac{f_{\text{cat,feed}}\,\rho}{\tau} - \dfrac{1}{\tau}C_{\text{cat}}$	(Catalyst)
$\dfrac{dC_1^*}{dt} = \dfrac{f_{\text{cat,feed}} f_{C_1^*,\text{cat}}\,\rho E_{\text{cat}}}{\tau}\dfrac{\text{WFMe}}{\text{MWMe}} - \dfrac{1}{\tau}C_1^* - C_1^*\left(\sum_i k_{st,M_i,1}C_{M_i}f_{\text{sorpt}} + k_{spd}\right)$	(Site 1)
$\dfrac{dC_2^*}{dt} = \dfrac{f_{\text{cat,feed}} f_{C_2^*,\text{cat}}\,\rho E_{\text{cat}}}{\tau}\dfrac{\text{WFMe}}{\text{MWMe}} - \dfrac{1}{\tau}C_2^* + C_1^*\sum_i k_{st,M_i,1}C_{M_i}f_{\text{sorpt}} - C_2^*\left(\sum_i k_{st,M_i,2}C_{M_i}f_{\text{sorpt}} + k_{spd}\right)$	(Site 2)
$\dfrac{dC_3^*}{dt} = \dfrac{f_{\text{cat,feed}} f_{C_3^*,\text{cat}}\,\rho E_{\text{cat}}}{\tau}\dfrac{\text{WFMe}}{\text{MWME}} - \dfrac{1}{\tau}C_3^* + C_2^*\sum_i k_{st,M_i,2}C_{M_i}f_{\text{sorpt}} - C_3^*\left(\sum_i k_{\text{act},\boldsymbol{M}_i}C_{M_i}f_{\text{sorpt}} + k_{spd}\right)$	(Site 3)
$\dfrac{dP_0^*}{dt} = \dfrac{f_{\text{cat,feed}} f_{P_0^*,\text{cat}}\,\rho E_{\text{cat}}}{\tau}\dfrac{\text{WFMe}}{\text{MWMe}} - \dfrac{1}{\tau}P_0^* + C_3^*\sum_i k_{\text{act},M_i}C_{M_i}f_{\text{sorpt}} - P_0^*\left(\sum_i k_{\text{ini},\boldsymbol{M}_i}C_{M_i}f_{\text{sorpt}} + k_{spd}\right)$	(Vacant Sites)
$\dfrac{dP_{E_i}^*}{dt} = -\dfrac{1}{\tau}P_{E_i}^* + P_0^* k_{\text{ini},M_i}C_{M_i}f_{\text{sorpt}} + \sum_{j\neq i}P_{E_j}^* k_{p,M_i,E_j}C_{M_i}f_{\text{sorpt}} - P_{E_i}^*\left(\sum_{j\neq i}(k_{p,M_j,E_i}C_{M_j}f_{\text{sorpt}}) + k_{spd}\right)$	(Growing Chains)
$\dfrac{dC_{M_i}}{dt} = \dfrac{f_{M_i,\text{feed}}\,\rho}{\tau M_{M_i}} - \dfrac{1}{\tau}C_{M_i} - C_{M_i}f_{\text{sorpt}}\left(k_{\text{act},\boldsymbol{M}_i}C_3^* + k_{\text{ini},\boldsymbol{M}_i}P_0^* + \sum_j k_{p,M_i,E_j}P_{E_j}^*\right)$	(Monomer)
$\quad - C_{M_i}f_{\text{sorpt}}(k_{st,M_i,1}C_1^* + k_{st,M_i,2}C_2^*)$	
$\dfrac{dT}{dt} = \dfrac{C_p^{\text{feed}}}{C_p\tau}(T_{\text{feed}} - T_{\text{ref}}) - \dfrac{1}{\tau}(T - T_{\text{ref}}) - \dfrac{hA}{\rho C_p V}(T - T_c) - \dfrac{1}{\rho C_p}\sum_i\sum_j k_{p,M_i,E_j}P_{E_j}^* C_{M_i}f_{\text{sorpt}}\Delta H_{\text{poly},M_i}$	(Energy)

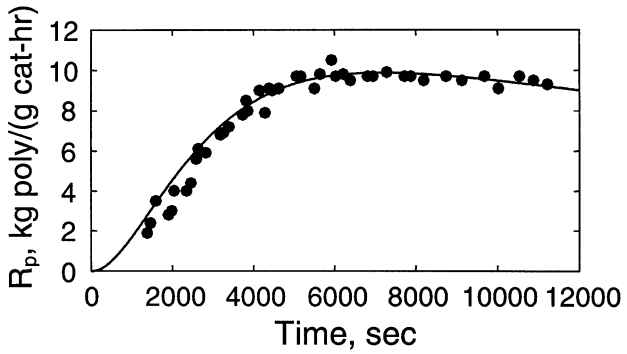

Figure 4. Comparison of model to data of McDaniel and Martin (1991) for polyethylene production with a chromium oxide catalyst on silica.

of catalyst feed fraction. Only polymer yield is affected by such a change in activity.

Base cases

As noted earlier, the major differences between the loop and tank reactors are the heat-transfer characteristics. In order to explore the effects of these and other parameters, base cases are chosen for representing typical loop- and tank-reactor designs and are given in Table 9. Note that the heat-transfer coefficient for the loop reactor was chosen to be twice that of the tank reactor to account for the increase in heat-transfer rate caused by fluid motion in the tubes of the loop reactor.

Table 6. Kinetic Parameters Used for HDPE Production Catalyzed by Chromium Oxide on Silica*

Activation Energies (cal/mol)	Value
Deactivation	12,000
All others	9,000
Preexponential Factors	**Value**
Site Transformations ($L/mol\cdot s$)	
$1 \rightarrow 2$ by ethylene	74.0
$1 \rightarrow 2$ by hexene	74.0
$2 \rightarrow 3$ by ethylene	74.0
$2 \rightarrow 3$ by hexene	74.0
Chain initiation ($L/mol\cdot s$)	
By ethylene	6.45×10^7
By hexene	6.45×10^7
Chain propagation ($L/mol\cdot s$)	
By ethylene, ethylene end group	1.21×10^9
By ethylene, hexene end group	5.40×10^{10}
By hexene, ethylene end group	1.21×10^9
By hexene, hexene end group	0.00
Site deactivation (s^{-1})	
Spontaneous	200

*Rate-constant parameters for chain initiation, propagation, and deactivation were initialized using reasonable values from available literature and modified to fit the specific rate curve measured by McDaniel and Martin (1991).

Reactor Dynamics for Decay-Type Catalysts

Loop reactors

Figures 5 and 6 illustrate the effect of catalyst residence time on the temperature and fractional ethylene conversion in a loop reactor for HDPE production using $TiCl_4$ catalysts on silica. Here we assume that the catalyst concentration in the exit stream is the same as that of the reactor contents so that the slurry residence time is the same as catalyst residence time. This is equivalent to assuming that the slurry is

Table 7. Constant Values Used in Simulations

Parameter	Value
Feed temperature (T_f, °C)	45.0
Reference temperature (T_{ref}, °C)	25.0
Ethylene heat of polymerization ($\Delta H_{poly,ethylene}$, cal/mol)	−24,800
Hexene heat of polymerization ($\Delta H_{poly,hexene}$, cal/mol)	−20,000
Ethylene feed fraction ($f_{eth,feed}$, wt basis)	0.420
Hexene feed fraction ($f_{hex,feed}$, wt basis)	0.017
Cocatalyst feed fraction ($f_{coc,feed}$, wt basis, $TiCl_4$ only)	2.5×10^{-3}
Hydrogen feed fraction ($f_{H,feed}$, wt basis, $TiCl_4$ only)	9.8×10^{-5}
Titanium metal weight fraction in catalyst (WFMe)	0.02
Chromium metal weight fraction in catalyst (WFMe)	0.01
Titanium molecular weight (MWMe)	47.9
Chromium molecular weight (MWMe)	52.0
Sorption factor (f_{sorpt})	0.5
Fraction of chromium catalyst feed of site type 1 ($f_{C_1^*,cat}$)	1
Fraction of deactivated titanium catalyst feed ($f_{dead,cat}$)	0.04
Fraction of titanium catalyst feed of type 1 ($f^1_{0,feed}$)	0.48
Fraction of titanium catalyst feed of type 2 ($f^2_{0,feed}$)	0.48
Molecular weight of ethylene ($M_{ethylene}$, monomer 1)	28.05
Molecular weight of hexene (M_{hexene}, monomer 2)	84.00
Molecular weight of triethyl aluminum cocatalyst (M_{coc})	198.3
Molecular weight of hydrogen (M_H)	2.0
Titanium catalyst activity (E_{cat}, mol sites/mol metal)	0.47
Chromium catalyst activity (E_{cat}, mol sites/mol metal)	0.30
Reference heat-transfer coefficient [h_0, cal/(cm^2·s·K)]	0.015

Table 8. Density and Heat-Capacity Correlation Coefficients

Quantity*	A	B	C	D
$\rho_{isobutane}$	0.6278	-1.394×10^{-3}	-6.144×10^{-5}	0
$\rho_{ethylene}$	0.6278	-1.394×10^{-3}	-6.144×10^{-5}	0
ρ_{hexene}	0.7048	-7.166×10^{-4}	-2.705×10^{-6}	0
$\rho_{polymer}$	0.9400	0	0	0
$C_{p,isobutane}$	0.4864	-5.320×10^{-3}	-7.987×10^{-5}	5.484×10^{-7}
$C_{p,ethylene}$	0.4864	-5.320×10^{-3}	-7.987×10^{-5}	5.484×10^{-7}
$C_{p,hexene}$	0.4864	-5.320×10^{-3}	-7.987×10^{-5}	5.484×10^{-7}
$C_{p,polymer}$	0.3369	2.420×10^{-3}	0	0

*The following equations are used to compute the pure-component heat capacities and densites for component i:
$C_{p,i} = A_i + B_iT + C_iT^2 + D_iT^3$, where $C_{p,i}$ [=] cal/(g °C), T [=] °C.
$\rho_i = A_i + B_iT + C_iT^2 + D_iT^3$, where ρ_i [=] g/cm^3, T [=] °C.

uniform throughout the reactor. The bifurcation diagram shows that, for a typical catalyst feed fraction of 3×10^{-5}, oscillatory steady states (denoted by a dashed line) exist over a wide range in residence time. Included in the range of oscillations is a residence time of 1 h, a typical value used in industrial loop reactors. Such oscillations can have a large impact on the operation of these processes, since final product properties are highly dependent on operating conditions. Temperature is especially important to reactor operation, and will therefore be used as the dependent variable for most bifurcation results presented.

If a transition is made from a steady state at 2 h of residence time (state A in Figures 5 and 6) to a steady state at 1 h of residence time (state B in Figures 5 and 6), the reactor system will begin to exhibit sustained oscillations. These oscillations, shown in Figure 7, have a period of about 40 min, and the maximum amplitude in temperature exceeds the process constraints defined by the diluent boiling point and polymer melting point. Thus, these are not feasible operating

Table 9. Base Cases Used in Loop and Tank Simulations

Quantity	Loop	Tank
Heat-transfer area per volume (A/V, cm^2/L)	65	20
Scaled heat-transfer coefficient (h/h_0)*	1	0.5

*The value of h_0 used in these simulations is 0.0150 cal/(cm^2·s·K).

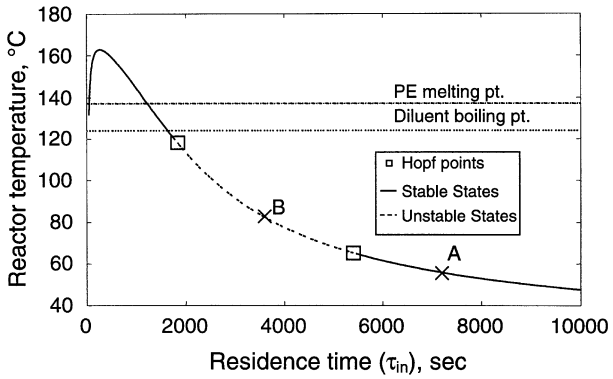

Figure 5. Effect of residence time in loop reactors for HDPE production catalyzed by $TiCl_4$ on silica.
$h/h_0^*(A/V) = 65$ cm^2/L; $f_{cat,feed} = 3\times10^{-5}$.

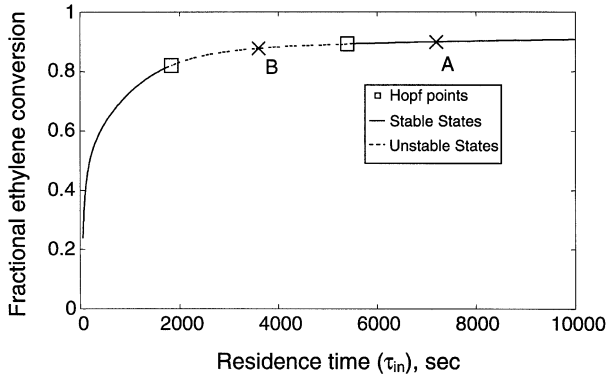

Figure 6. Effect of residence time on ethylene conversion in loop reactors for HDPE production catalyzed by $TiCl_4$ on silica.
$h/h_0^*(A/V) = 65$ cm^2/L; $f_{cat,feed} = 3\times10^{-5}$.

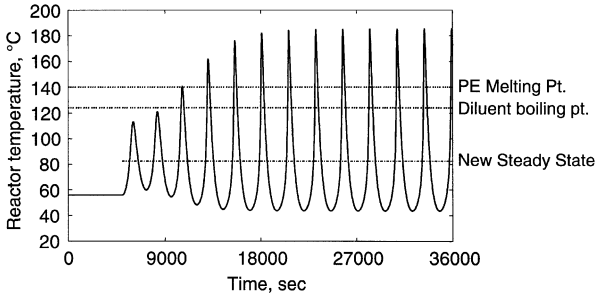

Figure 7. Sustained oscillations in the loop reactor system catalyzed by $TiCl_4$ on silica.
The change in residence time from $\tau_{in} = 7{,}200$ s to $\tau_{in} = 3{,}600$ s was made after 5,000 s elapsed. $f_{cat,feed} = 3.0\times10^{-5}$; $h/h_0^*(A/V) = 65$ cm^2/L.

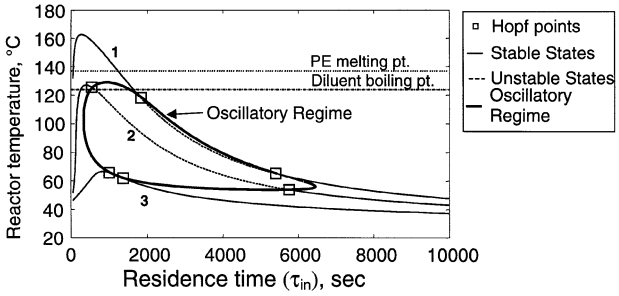

Figure 8. Effect of residence time and catalyst feed fraction on reactor temperature for the loop reactor catalyzed by $TiCl_4$ on silica ($h/h_0^*(A/V) = 65\ cm^2/L$).

Curves: (1) $f_{cat,feed} = 3.0\times10^{-5}$, (2) $f_{cat,feed} = 1.0\times10^{-5}$, (3) $f_{cat,feed} = 0.5\times10^{-5}$.

conditions for this reactor.

Figure 8 illustrates the effect of catalyst feed fraction on the region of oscillations for the loop reactor. Three separate bifurcation curves are shown for catalyst feed fractions of 0.5×10^{-5}, 1.0×10^{-5}, and 3.0×10^{-5}. Also shown is the locus of the Hopf bifurcation points (the open squares) as the catalyst feed fraction varies. Inside of the locus of Hopf points is the region of steady states about which oscillations can occur. It should be noted that the magnitude of oscillations can easily lie outside of the envelope created by the locus of Hopf points, but the steady states about which the system oscillates lie inside the envelope. As can be seen from Figure 8, this envelope is large in terms of both residence time and catalyst feed fraction. However, oscillations cease to exist for the loop reactor at catalyst feed fractions greater than 4.0×10^{-5}.

Comparison of loop and tank reactors

Figure 9 illustrates the effect of both catalyst feed fraction and heat transfer area per unit volume for HDPE production using $TiCl_4$ catalysts on silica at a residence time of 1 h. The base cases for both the tank and loop reactors are marked on this graph with crosses. Using the appropriate values of heat-transfer area per volume, heat-transfer coefficient, or catalyst feed fraction, the dynamic behavior can also be determined for other reactors of interest. Lines of constant operating temperature (80, 90 and 100°C) and constant polymer yield (kg polymer/g catalyst) are also shown in Figure 9, as is the locus of Hopf bifurcation points, indicating the regime where oscillations can occur. As can be seen from this graph, oscillations are unlikely for most operating conditions in tank reactors. Since the dynamics of tank reactors for HDPE production using $TiCl_4$ catalysts on silica are relatively uninteresting, no bifurcation plots for this system are presented here. However, it can be seen that the base case for the loop reactor using this catalyst lies well within the oscillatory regime. Thus, small changes in the reactor's heat-transfer characteristics or in catalyst feed fraction will not move operation out of the oscillatory regime. However, at larger catalyst feed fractions, nonoscillatory operation can be achieved at the expense of polymer yield.

To assess the effect of increasing throughput, the analogous plot for a residence time of 45 min is given in Figure 10.

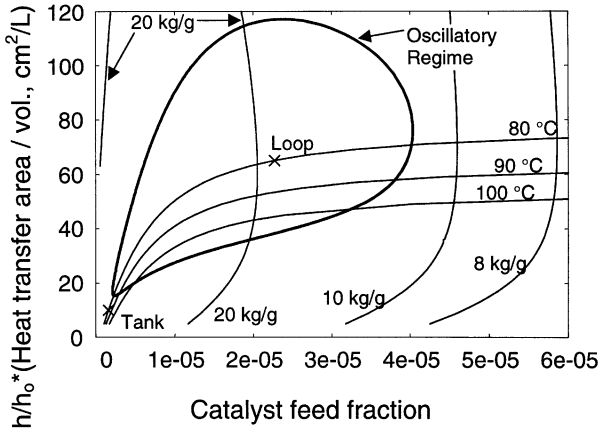

Figure 9. Effect of both heat-transfer area per volume and catalyst feed fraction for HDPE production catalyzed by $TiCl_4$ on silica at a residence time (τ_{in}) of 1 h.

Curves labeled with units of kg/g are polymer yield in terms of kg polymer produced per gram of catalyst. Temperature labels refer to curves of constant vessel temperature. *Note:* $h_0 = 0.015$ cal/(cm$^2\cdot$K$\cdot$s).

As can be seen, for the base case of loop reactors operating at both 80°C and 90°C, steady states lie within the oscillatory regime. Even higher values of catalyst feed fraction are required to escape the region where oscillations can occur. The tank reactor still lies outside of the oscillatory regime at these conditions.

Reactor Dynamics for Buildup-Type Catalysts

Loop reactors

Figure 11 shows the effect of residence time on the operation of HDPE production catalyzed by chromium oxide on

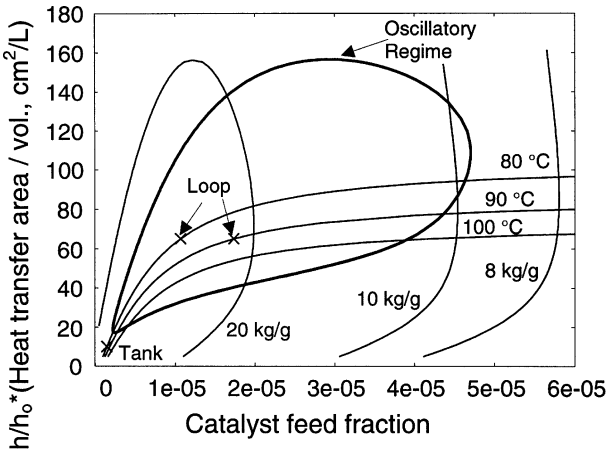

Figure 10. Effect of both heat-transfer area per unit volume and catalyst feed fraction on HDPE production catalyzed by $TiCl_4$ on silica for a residence time (τ_{in}) of 45 min.

Curves labeled with units of kg/g are polymer yield in terms of kg polymer produced per gram of catalyst. Temperature labels refer to curves of constant vessel temperature. *Note:* $h_0 = 0.015$ cal/(cm$^2\cdot$K$\cdot$s).

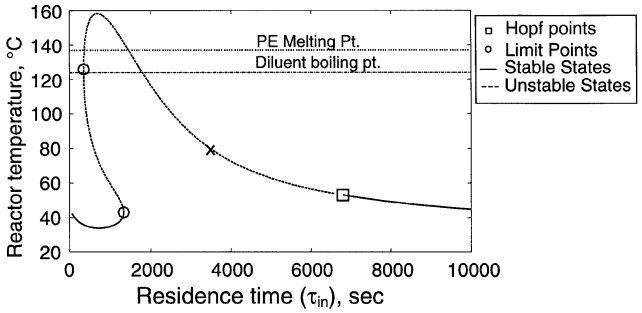

Figure 11. Effect of residence time in loop reactors for HDPE production catalyzed by chromium oxide on silica.

$h/h_0^*(A/V) = 65$ cm^2/L, $f_{cat,feed} = 4.5\times10^{-5}$.

silica in a slurry loop reactor. As can be seen, there are regions of both multiple steady states (between limit points) and oscillatory states (between the Hopf point and the limit point). The oscillations occur in the normal operating range of residence time, but multiple steady states would be seen only below residence times of about 20 min. For the unstable state marked with a cross in Figure 11, the system will exhibit sustained oscillations of large magnitudes shown in Figure 12 (far exceeding polymer melting point and diluent boiling point).

Figure 13 illustrates the effect of catalyst feed fraction on the bifurcation diagram for the loop reactor. Three continuation curves are plotted at catalyst feed fractions of 2.15×10^{-5}, 2.5×10^{-5}, and 4.5×10^{-5}. It can be seen that the region of multiple steady states stretches to include longer residence times as the catalyst feed fraction is decreased from 4.5×10^{-5} to 2.5×10^{-5}. However, if the catalyst feed fraction is further reduced, the bifurcation curve "pinches" and an isolated solution branch (isola) is formed. It is interesting to recall that regions of multiple steady states and isola were absent in the bifurcation diagrams for the decay-type catalysts. The range of residence times at which these multiplicity phenomena occur is in the same range as the sigmoidal character of the buildup-type catalyst activity curve given in Figure 4. Thus, it is postulated that these effects are due to the sigmoidal characteristics of the catalyst activity profile.

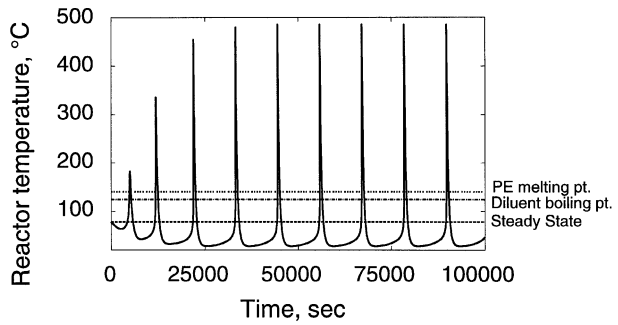

Figure 12. Oscillations exhibited in a loop-reactor system for HDPE production catalyzed by chromium oxide on silica for the steady state marked in Figure 11.

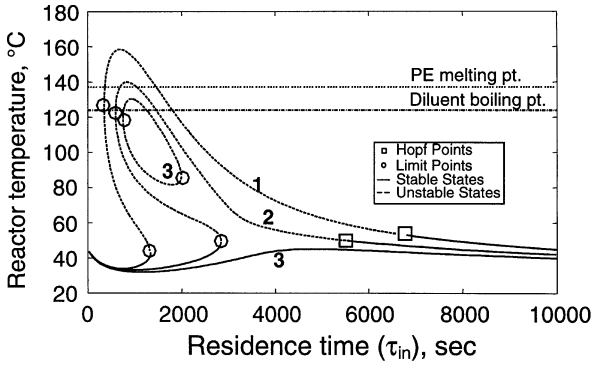

Figure 13. Effect of residence time and catalyst feed fraction on reactor temperature for the loop reactor using a chromium oxide catalyst on silica ($h/h_0^*(A/V) = 65$ cm^2/L).

Curves: (1) $f_{cat,feed} = 4.5\times10^{-5}$; (2) $f_{cat,feed} = 2.5\times10^{-5}$; (3) $f_{cat,feed} = 2.15\times10^{-5}$.

Tank reactors

Figures 14 and 15 illustrate the effect of residence time on temperature and fractional ethylene conversion in a slurry tank reactor at a catalyst feed fraction of 2.0×10^{-6}. As in the case of the tubular loop reactor, there is a region of multiplicity as well as an oscillatory region. In this case, multiple steady states can occur at residence times between 1 and 1.5 h, while oscillatory states can occur for residence times up to 7 h.

To illustrate the dynamic behavior of the reactor at the unstable middle steady state, simulations were run with positive and negative disturbances in residence time after the reactor was controlled for 10,000 s at the steady state marked in Figures 14 and 15. Figure 16 shows the dynamic response of the tank reactor temperature after the controller is turned off and the residence time is disturbed from 5,000 to 4,900 s. The reactor temperature slowly moves in a monotonic fashion from the middle steady state at 70°C to the lower steady state at 47°C. By contrast, Figure 17 shows the dynamic temperature response of the tank reactor when the residence time

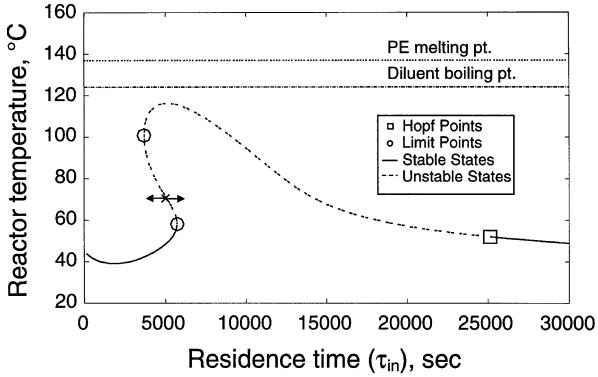

Figure 14. Effect of residence time on behavior of tank reactors for HDPE production catalyzed by chromium oxide on silica.

$h/h_0^*(A/V) = 10$ cm^2/L; $f_{cat,feed} = 2.0\times10^{-6}$.

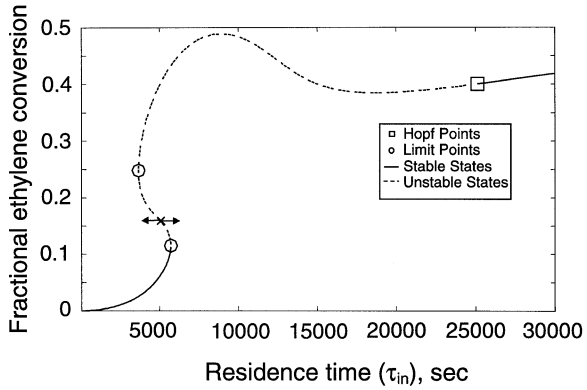

Figure 15. Effect of residence time on ethylene conversion in tank reactors for HDPE production catalyzed by chromium oxide on silica.

$h/h_0^*(A/V) = 10$ cm^2/L, $f_{cat,feed} = 2 \times 10^{-6}$.

is increased by 100 s. As can be seen, the reactor originally is driven toward the upper steady state, but ultimately settles to the lower steady state. However, this transient is very dangerous to reactor operation because the polymer melting point and diluent boiling point are exceeded for a significant time period, leading to serious reactor operation problems.

When a larger positive disturbance is made in reactor residence time, namely from 5,000 s to 6,000 s, the reactor exits the region of multiplicity and enters the region of oscillatory behavior. This oscillatory behavior is exhibited by the dynamic response depicted in Figure 18. Again, the reactor exceeds diluent boiling point and polymer melting point for a significant period of time during these oscillations, leading to infeasible reactor conditions.

Figure 19 shows the change in the bifurcation diagram for the tank reactor when the catalyst feed fraction is varied. Similar to the loop case, an isola is formed as the catalyst feed fraction is decreased. Again, the region of multiplicity extends to larger residence times before the curve "pinches" and forms the isola. As in the loop case, the region of multiplicity lies in approximately the first 5,000 s of residence time —the same time frame as the sigmoidal part of the buildup catalyst activity profile of Figure 4.

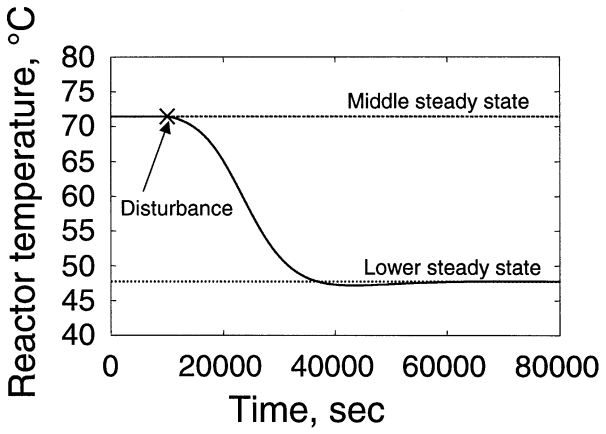

Figure 16. Dynamic response of tank system for HDPE production catalyzed by chromium oxide on silica around an unstable steady state.

A negative change in residence time (τ_{in}) of 100 s was made at the indicated point.

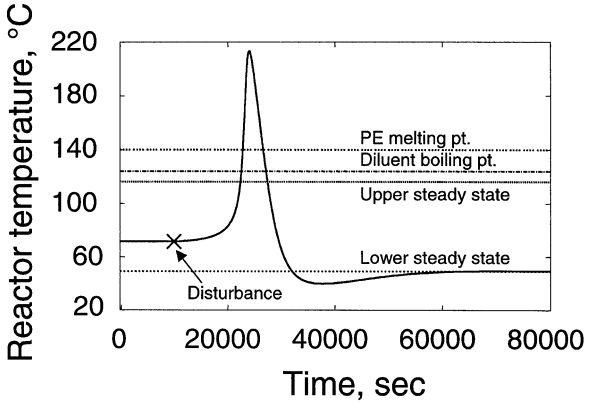

Figure 17. Illustration of unstable dynamic behavior of a tank system for HDPE production catalyzed by chromium oxide on silica in a tank reactor.

A positive change in residence time (τ_{in}) of 100 s was made at the indicated point.

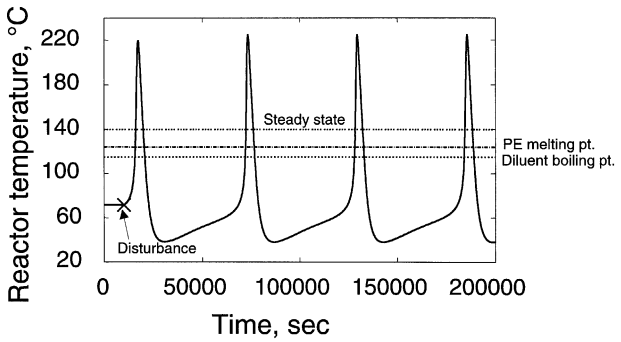

Figure 18. Oscillations in tank reactors for HDPE production catalyzed by chromium oxide on silica.

A positive change in residence time (τ_{in}) of 1,000 s was made at the indicated point.

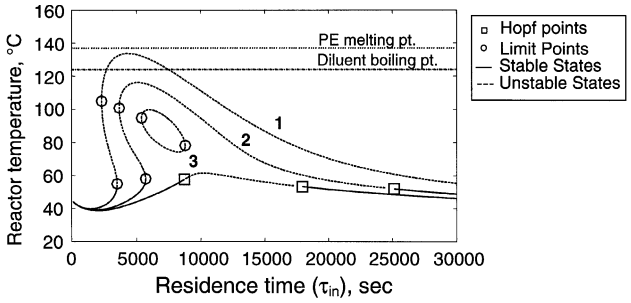

Figure 19. Effect of residence time and catalyst feed fraction on reactor temperature for the tank reactor catalyzed by chromium oxide on silica ($h/h_0^*(A/V) = 10$ cm^2/L).

Curves: (1) $f_{cat,feed} = 2.5 \times 10^{-6}$; (2) $f_{cat,feed} = 2.0 \times 10^{-6}$; (3) $f_{cat,feed} = 1.83 \times 10^{-6}$.

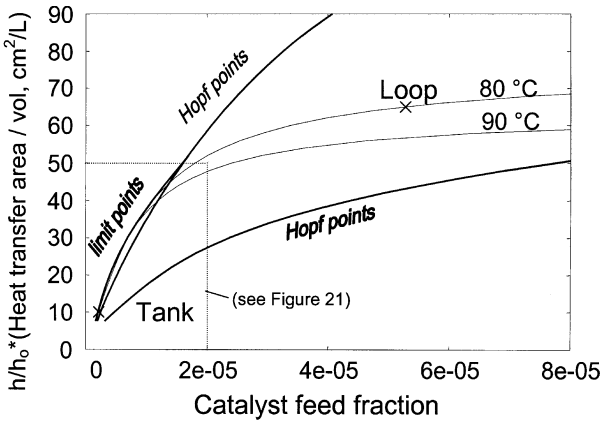

Figure 20. Effect of catalyst feed fraction and heat-transfer area per volume on system dynamics for HDPE production catalyzed by chromium oxide on silica using a coolant temperature of 25°C and one hour of residence time (τ_{in}).

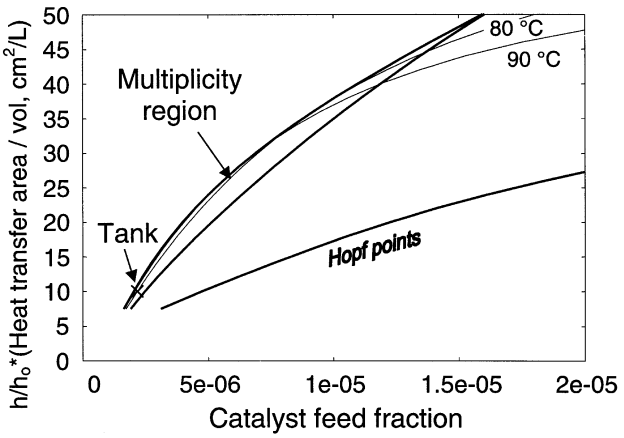

Figure 21. Closer look at the region of multiplicity for HDPE production using chromium oxide catalysts on silica.

T_c = 25°C, one hour residence time (τ_{in}).

Comparison of loop and tank reactors

Figure 20 shows the effect of both heat-transfer area per unit volume and catalyst feed fraction for a coolant temperature of 25°C and 1 h of residence time. Base cases for the loop and tank reactors are marked with crosses. Lines of constant operating temperature at 80 and 90°C are plotted, as are the loci of Hopf and limit points. Inside the region bounded by the limitpoint curves, the reactor can exhibit multiplicity phenomena. Inside the region bounded by Hopf points, the system can exhibit oscillations. Note that the base case for loop-reactor operation lies well within the region of oscillations. The region of multiplicity is more easily examined from the expanded view given in Figure 21, which shows that the base case for tank operation lies just inside the region of multiplicity for a residence time of 1 h and a coolant temperature of 25°C. The loop-reactor base case is well outside the region of multiplicity.

The simulations run at coolant temperatures of 25°C were carried out for the chromium oxide catalyst on silica to provide a means of comparison between systems with buildup- and decay-type rate profiles. However, since industrial operation HDPE production using this catalyst is often carried out at higher coolant temperatures, the effect of this elevated temperature on the dynamic behavior is of interest. Figure 22 shows a plot of the dynamic behavior as a function of catalyst feed fraction and heat-transfer area per volume at a residence time of 1 h and an elevated coolant temperature of 50°C. This elevated temperature causes a significant change in the energy balance and, subsequently, in the dynamic behavior. As can be seen in Figure 22, there is no multiplicity region for a coolant temperature of 50°C. However, the base loop and tank cases remain in the oscillatory regime for operating temperatures between 80 and 100°C. As the coolant temperature is further increased to 75°C, the nature of the system dynamics changes further, as is shown in Figure 23. In this case, both loop and tank operation lie outside of the oscillatory regime. A coolant temperature of 75°C is used in the industrial operation of some HDPE production processes using chromium oxide catalysts on silica. Such high coolant temperatures are required to maintain tight temperature control of the reactor since this is the major method of controlling the melt index of the polymer produced using some older catalysts. For newer catalysts that are sensitive to chain-transfer agents, lower coolant temperatures can be used in order to increase production rates. However, as Figures 20–23 show, this brings with it more complex dynamic behavior for the reactor.

Conclusions

Dynamic analysis of slurry tank and loop reactors for HDPE production using a $TiCl_4$ catalyst on silica that exhibits a de-

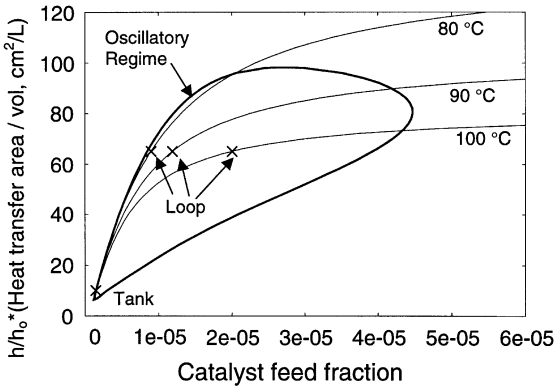

Figure 22. Effect of catalyst feed fraction and heat-transfer area per volume on system dynamics for HDPE production catalyzed by chromium oxide on silica using a coolant temperature of 50°C and one hour of residence time (τ_{in}).

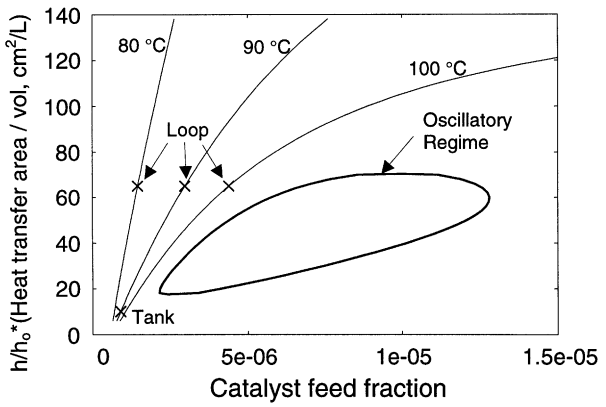

Figure 23. Effect of catalyst feed fraction and heat-transfer area per volume on system dynamics for HDPE production catalyzed by chromium oxide on silica using a coolant temperature of 75°C and one hour of residence time (τ_{in}).

cay-type activity profile shows that loop reactors can exhibit oscillatory behavior under conditions typically found in industrial use. These oscillations can cause the reactor to exceed temperature constraints such as polymer melting point and diluent boiling point. The oscillations disappear at high catalyst feed rates. Tank reactors using $TiCl_4$ catalysts on silica for HDPE production do not show oscillatory behavior under normal operating conditions. Multiple steady states are not expected for these Ziegler-Natta catalysts.

By contrast, for a chromium oxide catalyst with a buildup activity profile, both loop and tank reactors can exhibit oscillations, steady-state multiplicity, and isolated solution branches (isola) over a wide range of operating conditions. High feed rates of the chromium oxide catalyst can cause steady-state multiplicity and isola to disappear for both loop and tank reactors. Dynamic transitions and sustained oscillations observed for the buildup-type catalyst can cause both loop- and tank-reactor temperatures to exceed diluent boiling-point and polymer melting-point constraints. The multiplicity and isola phenomena experienced for this catalyst system occur for residence times in the same time frame as the buildup period in catalyst activity. Thus, it is hypothesized that the buildup nature of the catalyst activity profile is the cause for this behavior. When higher coolant temperatures are used for the chromium oxide catalyzed reactors to facilitate melt index control, both oscillations and multiplicity phenomena disappear. However, reactor productivity is greatly decreased under these conditions.

Acknowledgments

The authors are indebted to the industrial sponsors of the University of Wisconsin Polymer Reaction Engineering Laboratory and to the U.S. Department of Energy for financial support. We also thank Príamo Melo, Shreyas Chakravarti, Dennis Lo, Carlos Villa, Sanjeev Naik, and Pavel Pinkas for their insight and support.

Notation

A = heat transfer area, cm^2
C_i^* = concentration of chromium site type i, mol/L
C_B = concentration of byproduct, mol/L
C_{cat} = concentration of catalyst, g/L
C_{cocat} = concentration of cocatalyst, mol/L
C_d = concentration of deactivated catalyst sites, mol/L
C_H = concentration of hydrogen, mol/L
C_{M_i} = concentration of monomer M_i in the slurry, mol/L
$C_{M_i,effective}$ = concentration of monomer M_i at the catalyst site, mol/L
C_p = heat capacity of the reaction mixture, cal/(g·K)
C_p^{feed} = heat capacity of the feed stream, cal/(g·K)
C_{pot} = concentration of potential catalyst sites, mol/L
D_{n,E_i}^k = concentration of dead polymer chains of chain length n, site type k, and monomer end group E_i, mol/L
E_{cat} = catalyst activity, mol sites/mol metal
$E_{cat,0}$ = base value for the catalyst activity, mol sites/g catalyst
$f_{0,feed}^k$ = fraction of vacant sites in the catalyst feed, dimensionless
$f_{c_i^*,cat}$ = fraction of chromium site type i in catalyst feed, dimensionless
$f_{cat,feed}$ = weight fraction of catalyst in the feed, dimensionless
$f_{coc,feed}$ = weight fraction of cocatalyst in the feed, dimensionless
$f_{dead,cat}$ = fraction of catalyst fed to the reactor that is already deactivated, dimensionless
f_{sorpt} = fraction of bulk species concentration that is available at the monomer site, dimensionless
h = heat-transfer coefficient, cal/(cm^2·s·K)
h_0 = base value of the heat-transfer coefficient, cal/(cm^2·s·K)
$k_{act,cocat}^k$ = rate constant for the activation of catalyst sites of type k by cocatalyst, L/(mol·s)
k_{act,M_i}^k = rate constant for the activation of site type k by monomer M_i, L/(mol·s)
k_{init,M_i}^k = rate constant for initiation of chains of site type k by monomer M_i, L/(mol·s)
k_{p,M_i,E_j}^k = rate constant for polymerization on site type k by adding monomer M_i to an end group of type E_j, L/(mol·s)
k_{spd} = rate constant for spontaneous catalyst deactivation, s^{-1}
$k_{st,M_i,j}$ = rate constant for site transformation of a chromium site of type j to one of type $j+1$ by monomer M_i, L/(mol·s)
$k_{tr,cocat,E_i}^k$ = rate constant for chain transfer to cocatalyst on site type k with an end group E_i, L/(mol·s)
k_{tr,H,E_i}^k = rate constant for chain transfer to hydrogen on site type k with end group E_i, L/(mol·s)
k_{tr,M_j,E_i}^k = rate constant for chain transfer to monomer M_j on site type k with end group E_i, L/(mol·s^{-1})
k_{tr,sp,E_i}^k = rate constant for the spontaneous chain transfer on site type k with end group E_i, s^{-1}
M_{cocat} = molecular weight of cocatalyst, g/mol
M_H = molecular weight of hydrogen, g/mol
M_{M_i} = molecular weight of monomer M_i, g/mol
MWMe = molecular weight of metal in catalyst, g/mol
P_{act,E_i}^k = concentration of growing polymer chains of site type k and monomer end group E_i, mol/L (used for balance equations with the $TiCl_4$ catalyst on silica)
P_{n,E_i}^k = concentration of growing polymer chains of chain length n, site type k, and monomer end group E_i, mol/L (used for the $TiCl_4$-on-silica catalyst reaction mechanism)
$P_{E_i}^*$ = concentration of growing polymer chains with monomer end group E_i, mol/L (used for balance equations with the chromium oxide catalyst on silica)
P_{n,E_i}^* = concentration of growing polymer chains of chain length n and monomer end group E_i, mol/L (used for the reaction mechanism for chromium oxide catalysts on silica)
P_0^k = concentration of vacant titanium catalyst sites of type k, mol/L
P_0^* = concentration of vacant chromium catalyst sites, mol/L

Q = outlet volumetric flow rate, L/s
Q_{in} = inlet volumetric flow rate, L/s
R = universal gas constant, 1.987 cal/(mol·K)
T = reactor temperature, °C
T_c = coolant temperature, °C
T_{feed} = temperature of the feed, °C
T_{ref} = reference temperature for energy balance, °C
t = time, s
V = reactor volume, L
WFMe = weight fraction of metal in catalyst, dimensionless

Greek letters

$\Delta H_{poly,M_i}$ = heat of polymerization for monomer M_i, cal/mol
ρ = density of the reactor contents, g/L
ρ_{in} = density of the feed stream mixture, g/L
τ = reactor residence time referenced to exit volumetric flow rate ($\tau = V/Q$), s
τ_{in} = reactor residence time referenced to inlet volumetric flow rate ($\tau_{in} = V/Q_{in}$), s

Literature Cited

Benham, E. A., M. P. McDaniel, R. R. McElvain, and R. O. Schneider, "High-Temperature Slurry Polymerization of Ethylene," U.S. Patent No. 5,071,927 (1991).

Calabro, D. C., and F. Y. Lo, "A Comparison of the Reaction Kinetics for the Homo- and Copolymerization of Ethylene and Hexene with a Heterogeneous Ziegler Catalyst," *Transition Metal Catalyzed Polymerizations*, R. P. Quirk, ed., Cambridge Univ. Press, Cambridge, p. 729 (1988).

Chandrasekhar, V., P. R. Srinivasan, and S. Sivaram, "Recent Developments in Ziegler-Natta Catalysts for Olefin Polymerization and Their Processes," *Indian J. of Technol.*, **26**, 53 (1988).

Choi, K. Y., and W. H. Ray, "The Dynamic Behaviour of Fluidized Bed Reactors for Solid Catalyzed Gas Phase Olefin Polymerization," *Chem. Eng. Sci.*, **40**, 2261 (1985).

Choi, K. Y., and W. H. Ray, "The Dynamic Behavior of Continuous Stirred-Bed Reactors for Solid Catalyzed Gas Phase Polymerization of Propylene," *Chem. Eng. Sci.*, **43**, 2587 (1988).

Debling, J. A., G. C. Han, F. Kuijpers, J. VerBurg, J. Zacca, and W. H. Ray, "Dynamic Modeling of Product Grade Transitions for Olefin Polymerization Processes," *AIChE J.*, **40**, 506 (1994).

Doedel, E., "AUTO: A Program for the Automatic Bifurcation Analysis of Autonomous Systems," *Proc. 10th Manitoba Conf. on Numerical Mathematics and Computing*, Univ. of Manitoba, Winnipeg, Man., Canada (1981).

Gorbach, A., S. D. Naik, and W. H. Ray, "Dynamics and Stability Analysis of Solid Catalyzed Gas Phase Polymerization of Olefins in Continuous Stirred Bed Reactors," *Chem. Eng. Sci.*, **55**, 4461 (2000).

Hogan, J. P., D. D. Norwood, and C. A. Ayers, "Phillips Petroleum Company Loop Reactor Polyethylene Technology," *J. Appl. Poly. Sci.: Appl. Poly. Symp.*, **36**, 49 (1981).

Hyanek, I., J. Zacca, F. Teymour, and W. H. Ray, "Dynamics and Stability of Polymerization Process Flow Sheets," *Ind. Eng. Chem. Res.*, **34**, 3872 (1995).

Kashiwa, N., and J. Yoshitake, "The Influence of the Valence State of Titanium in $MgCl_2$-Supported Titanium Catalysts on Olefin Polymerization, *Makromol. Chem.* **185**, 1133 (1984).

Keii, T., *Kinetics of Ziegler-Natta Polymerization*, Kodansha Scientific Books, Tokyo, p. 15 (1972).

Kissin, Y. V., "Olefin Polymers (Polyethylene)," *Kirk-Othmer Encyclopedia of Chemical Technology*, Vol. 17, 4th ed., Wiley, New York (1996).

Kosek, J., and Ray, W. H., "Dynamics and Stability of Slurry Olefin Polymerization Processes," *Récents Prog Génie Proc.*, **13**, 97 (1999).

Lemmon, W. E., M. O. McLinden, and D. G. Friend, "Thermophysical Properties of Fluid Systems," *NIST Chemistry WebBook, NIST Standard Reference Database Number 69*, National Institute of Standards and Technology, Gaithersburg, MD (http://webbook.nist.gov) (1998).

Liljenroth, F. G., "Starting and Stability Phenomena of Ammonia-Oxidation and Similar Reactions," *Chem. Metall. Eng.* **19**, 287 (1918).

McDaniel, M. P., "Supported Chromium Catalysts for Ethylene Polymerization," *Adv. Catal.*, **33**, 47 (1985).

McDaniel, M. P., and S. J. Martin, "Poisoning Studies on Cr/Silica. 2. Carbon Monoxide," *J. Phys. Chem.*, **95**, 3289 (1991).

Murakami, Y., T. Hirose, S. Ono, and T. Nishijima, "Mixing Properties in Loop Reactor," *J. Chem. Eng. Jpn.*, **15**, 121 (1982).

Natta, G., "Une Nouvelle Classe de Polymères d'α-Olefiens ayant une Régularité de Structure Exceptionnelle," *J. Polym. Sci.*, **16**, 143 (1955).

Norwood, D. D., "Control of Olefin Polymerization Reactions," U.S. Patent No. 3,257,362 (1966).

Nowak, U., and L. Weimann, "A Family of Newton Codes for Systems of Highly Nonlinear Equations," *Tech. Rep. TR-91-10*, Konrad-Zuse-Zentrum für Informationstechnik, Berlin (1991).

Osswald, T. A., and G. Menges, *Materials Science of Polymers for Engineers*, Hanser-Gardner, Munich, p. 35 (1995).

Petzold, L. R, "Description of DASSL: A Differential/Algebraic System Solver," *Tech. Rep. SAND82-8637*, Sandia National Laboratory, Livermore, CA (1982).

Ray, W. H., and C. M. Villa, "Nonlinear Dynamics Found in Polymerization Processes—A Review," *Chem. Eng. Sci.*, **55**, 275 (2000).

Storck, W. J, P. L. Short, M. McCoy, M. S. Reisch, A. M. Thayer, and J. Tremblay, "Facts and Figures for the Chemical Industry," *Chem. Eng. News*, **78**(26), 55 (2000).

Takeda, M, and W. H. Ray, "Optimal Grade Transition Strategies for Multistage Polyolefin Reactors, **45**, 1776 (1999).

Zacca, J. J., and W. H. Ray, "Modelling of the Liquid Phase Polymerization of Olefins in Loop Reactors," *Chem. Eng. Sci.*, **48**, 3743 (1993).

Zacca, J. J., *Distributed Parameter Modelling of the Polymerization of Olefins in Chemical Reactors*, PhD Thesis, Univ. of Wisconsin-Madison (1995).

Ziegler, K., "Directed Polymerization of Ethylene and Its Homologues," *Pet. Refiner*, **34**, 111 (1955).

Manuscript received Oct. 2, 2000, and revision received May 29, 2001.